Heliyon 10 (2024) e28255

Contents lists available at ScienceDirect

Heliyon

journal homepage: www.cell.com/heliyon

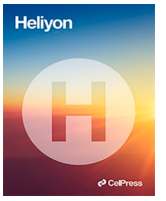

Research article

Thermal performance and experimental analysis of stainless steel flat plate solar collector with full-flow channels

Yi He [a], Hongwen Yu [a,*], Guangbin Duan [b], Yong Wang [b], Qianfu Yang [c], Lei Feng [c], Jiaming Zhang [d]

[a] The School of Architecture and Urban Planning, Shandong Jianzhu University, Jinan, 250101, China
[b] School of Materials Science and Engineering, University of Jinan, Jinan, 250024, China
[c] Shandong Sangle Group Co., Ltd, Jinan, 250101, China
[d] Zhongke Low Carbon Technology Co., Ltd, Jinan, 250014, China

ARTICLE INFO

Keywords:
Ultra-pure ferritic stainless steel
Flat plate solar collector
Full-flow channels
Microchannels

ABSTRACT

The thermal performance of a flat plate solar collector (FPSC) is a critical indicator that depends on the environment, operational parameters, and dimensions. This study examines the impact of size on thermal performance improvement mechanisms. Firstly, numerical simulation models are introduced as the foundation for optimization research. This involves analyzing the flow resistance of microchannels and defining their structural parameters. Furthermore, experimental tests were conducted on a stainless steel flat plate solar collector (S/S FPSC) with the best design parameters to validate the accuracy of the mathematical model during the design phase. The results indicate that increasing the width of the microchannel and the height of corrugations can effectively enhance the thermal performance of the S/S FPSC. The momentary efficiency is projected to reach a remarkable 86.10% under ideal circumstances. Additionally, a mathematical expression was proposed to establish the relationship between the surrounding conditions and the momentary efficiency of the S/S FPSC. Moreover, the microchannel comprises S/S material, maintaining a homogeneous temperature distribution to maximize heat absorption. The use of stainless steel also extends the lifespan of the FPSC.

1. Introduction

Solar thermal technology converts solar energy into thermal energy, establishing itself as one of the most commercially viable renewable energy technologies. Its high conversion efficiency is propelled by a combination of political and economic factors [1]. Approximately 50% of the world's energy consumption is thermal energy, and it is projected that one-third of this demand could be met or supplemented by solar energy [2]. This becomes particularly significant in the current global emphasis on carbon neutrality. Solar energy emerges as a capable solution to address buildings' hot water and heating needs, presenting a substantial market opportunity with significant development potential.

The solar collector stands as a pivotal component within the solar thermal system, offering various types tailored to meet diverse temperature requirements. These include flat-plate collectors, unglazed collectors, evacuated tube collectors, and concentrating solar collectors [3]. Among these, flat-plate collectors possess distinctive bearing strength and efficiency characteristics, making them

* Corresponding author.
E-mail address: hongwen_yu@163.com (H. Yu).

https://doi.org/10.1016/j.heliyon.2024.e28255
Received 1 December 2023; Received in revised form 14 March 2024; Accepted 14 March 2024
Available online 22 March 2024

highly suitable for applications in Building-Integrated Solar Thermal systems (BIST) [4]. Flat-plate collectors, integral to BIST, typically consist of four main elements: a transparent cover, collector core, channel system, and housing. Ongoing research aims to enhance heat collector performance by focusing on improving heating-collecting efficiency [5], medium heat transfer efficiency [6] and reducing heating loss [7]. To achieve these objectives, developers and researchers have devised various technical solutions. For instance, Giovannetti [8] investigated the impact of selective glass coatings on covers on solar irradiance. Mekhilef [9] utilized selective glass coatings to enhance the efficiency of heat collection. Jia [10] optimized the baffle structure to improve the thermal performance of spiral solar air heaters. Song [11] introduced a rectangular hole plate to enhance the performance of photovoltaic thermal solar air heaters. Sobhansarbandi [12] employed Phase Change Materials (PCMs) to increase the efficiency of heat transfer and improve the performance of the solar heater. Fernández [13] focused on optimizing the materials of collectors to minimize heating loss.

A solar energy-absorbing coating is applied to the surface of the collecting plate to facilitate the "light-heat transition". In contrast, the air/water/fluid channel on the back of the collector plate is responsible for heat transfer. Consequently, the design parameters of the collector play a crucial role in directly influencing the performance of solar thermal conversion and heat transfer. These design considerations encompass various factors, including the thermal conductivity of the plate core substrate [14], the thermal resistance of the contact between the substrate and the channel [15], as well as the arrangement [16] and geometry [17] of the channel. This includes features such as perforated fins and pebbles [18], which influence the uniformity of heat transfer within the medium flow.

In current research, significant optimization and innovation have been made in heat collectors. When considering the materials used for plate core substrates, options include copper, aluminum, and stainless steel. Diamantino [19] conducted investigations to assess the durability of selective solar absorber coatings under various environmental conditions. Considering the development demand for Building Integrated Photovoltaic (BIPV), collectors are expected to have a lifespan of at least 25 years or more [20]. In the realm of solar applications at medium to high temperatures, stainless steel (S/S) substrates have replaced traditional copper and aluminum substrates due to their enhanced durability [21]. Moreover, the market has witnessed the rapid introduction and commercialization of new materials, such as Ferrochrome oxide [22], Ni/NiO [23], Fe_2O_3 [24], and Co_3O_4 [25]. These materials have facilitated the widespread adoption of stainless steel-based collectors, particularly in concentrating collectors designed for medium and high-temperature applications. This reflects the continuous evolution of materials to meet the durability and performance demands of modern solar collectors.

Due to the various channel structures, there are significant differences in connection methods. Three types of channels—tube, wing, and snake-shaped—exist, each with distinct connection approaches. The linkage between the wick of the collector plate and the channel typically employs welding or rolling techniques [26]. While these methods reduce processing complexity, they also lead to an increase in thermal resistance. Channels, including flat box and micro-channel types, utilize the wick of the collector plate as the heat transfer medium [27]. In this design, the surface of the absorber features a photothermal conversion coating, while the interior serves as the heat transfer channel. This collector design offers the advantage of reducing thermal resistance and enhancing heat transfer efficiency between the heat-absorbing body and the heat-transfer medium. However, it also presents challenges, such as processing difficulties and increased pressure drop within the channel. Ma [28] modified a flat-plate solar water heater with an L-shaped fin collector to provide both hot water and air. Chong [29] proposed a V-trough solar water heater system with a low cost to achieve an optical efficiency of 70.54% or 1.41 suns. Kumar et al. [30] presented more detailed modifications to the solar thermal collector, exploring the effects of parametric variations of single discrete arc-shaped ribs on the Nusselt number, friction factor, and thermo-hydraulic performance as a means of optimization. Wang [31] designed two types of solar air collectors based on flat micro-heat pipe arrays to enhance efficiency through a significant volumetric flow rate of air. These diverse modifications showcase the ongoing efforts to optimize solar collector designs for improved efficiency and performance in various applications.

In the research about the flow path, Yu [32] conducted a study using a simulation program to investigate the impact of the arrangement of triangular baffles and the height of the air gap on the performance of an air-type PVT collector. Gholipour [33] introduced helical coil and spiral tube adsorbent tubes to increase the volumetric flow rate, thereby improving the performance of collectors. Kotb [34] optimized the number and arrangement of tubes, leading to a 41% reduction in initial cost while ensuring high-efficiency operation. These studies highlight the significance of flow path optimization in enhancing the overall performance and efficiency of solar collectors.

The collectors with S/S have gained widespread adoption in solar applications at medium to high temperatures, utilizing compound parabolic concentrating technology [35] to enhance solar irradiance and operating temperatures. They employ a straight-through evacuated collector structure [36]. In comparison to copper and aluminum, S/S exhibits a different level of thermal conductivity [37], not conforming to the exact theoretical estimation. Partha et al. [38] verified the possibility of superior heat transfer in corrugated aluminum alloy plate heat-transferring devices due to the high turbulence generated. When applying an S/S substrate to a non-concentrating flat plate collector, it becomes essential to enhance the heat transfer efficiency of the flow channel to achieve optimal system thermal performance. Gong [39] demonstrated that increasing the heat transfer area through microchannel structures can bridge the gap in substrate thermal conductivity. Jalil and Abdulkadhim [40] considered microchannel technology to improve heat transfer to flowing air, with good agreement between numerical results and experimental outcomes. Jalil et al. [41] experimentally investigated the cooling performance of microchannels manufactured from copper metal at different velocities and electric powers of the heater. These studies underscore the importance of optimizing heat transfer efficiency in the context of S/S-based collectors to achieve optimal thermal performance in various applications.

This study proposes a novel collector design incorporating microchannels within a full-flow plate featuring a stainless steel (S/S) substrate. This innovative approach introduces a new airflow configuration to enhance heat extraction. Our experiment aims to assess the impact of utilizing microchannel structures in air heat exchangers. Additionally, the use of S/S is intended to extend the collector's

operational lifespan and reduce maintenance costs.

The novelty of this experimental project lies in the use of a microchannel type of solar collector with S/S. This work has developed a mathematical model within a simulation program to optimize design parameters and ensure the finalization of the product design. Based on this practical model, this study will evaluate the thermal performance of the new collector through experiments. This integrated approach combines theoretical modeling with practical experimentation to validate and refine the collector design for improved efficiency and longevity.

Acronyms	
ASS	Austenitic Stainless Steel
BIST	Building-Integrated Solar Thermal Systems
BIPV	Building Integrated Photovoltaic
CFD	Computational Fluid Dynamics
FPSC	Flat Plate Solar Collector
NDTI	Normalized Difference Temperature Index
PMCs	Phase Change Materials
S/S	Stainless Steel
SSC	Solar Selective Coating
UFSS	Ultra-pure Ferritic Stainless Steel

Nomenclature	
α	Absorption
ρ	Density (kg/m^3)
f	Flow Resistance
C_p	Specific Heat Capacity (J/(kg K)
λ	Thermal Conductivity (W/m·K)
e	Thermal Emittance
ε	Turbulent Dissipation Rate
k	Turbulent Kinetic Energy

2. Numerical model formulation

2.1. Physical model

Building upon our previous research [42], this study designed a collector that incorporates microchannels within a full-flow plate. To evaluate its performance, this research developed a numerical model using computational fluid dynamics (CFD). The first aim is to determine whether the CFD results compare accurately with the experimental results. Then, this model enables us to analyze flow patterns and temperature distribution within the collector structure, facilitating the optimization of parameters for enhanced overall performance.

The microchannels in our design exhibit a compact and lightweight structure with superior heat transfer efficiency [43]. In comparison to traditional collectors, microchannels have fewer welding points and offer a larger heat exchange area, as depicted in Fig. 1. This design innovation is expected to contribute to improved efficiency and reduced weight compared to conventional collectors.

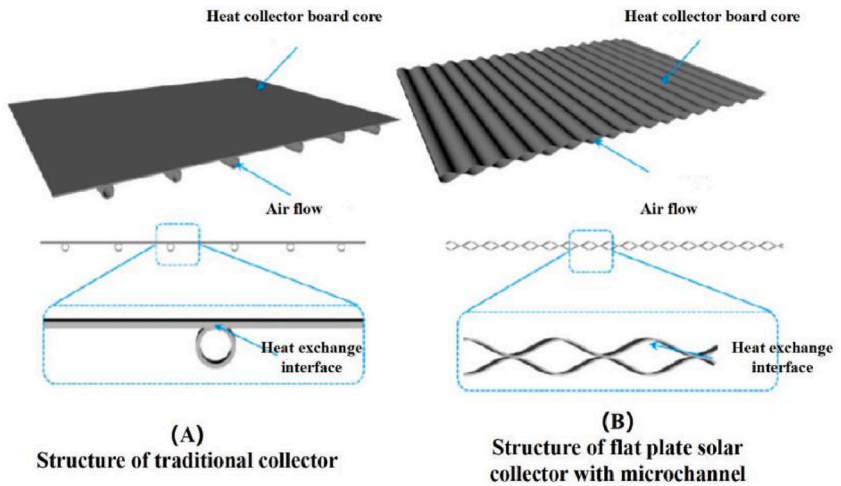

Fig. 1. Structure of collectors.

Next, Fig. 2 illustrates a stainless steel flat plate solar collector (S/S FPSC) featuring full-flow channels. The relevant parameters are clearly defined and labeled in Fig. 3. Specifically, L represents the space between adjacent microchannels, d signifies the welding line, R indicates the diameter of the microchannel (semi-minor axis), H represents the height of corrugation in the microchannel and the stamping depth of the microchannel, D denotes the width of the microchannel (semi-major axis).

The cross-sectional images of the microchannels exhibit an elliptical shape. Among these parameters, the diameter (R) plays a pivotal role in determining the cross-sectional area of the flow path. Furthermore, it significantly influences the heat exchange area and flow rate of the medium. The elliptical shape, defined by the diameter (R), is a key factor in shaping the characteristics of the microchannels and ultimately impacting the efficiency and performance of the collector.

The collector model was constructed using Gambit with the following dimensions: 800 mm × 2370 mm × 0.41 mm(length × width × thickness). In the simulation, the solar radiation intensity was set to 1000 W/m^2, the solar absorptance of the solar selective absorbing coating was 0.92, and the emissivity was 0.1. The 3D model is shown in Fig. 4. These simulation parameters provide a realistic representation of the collector's conditions and characteristics for accurate analysis and evaluation.

2.2. Parameters setup

(1) Collector Diameter: In this study, three sets of collector diameters were simulated, 6 mm, 7 mm, and 8 mm to analyze collector performance. The mesh generation was performed using Tet/Hybrid in TGrid, and an interval size of 3.5 was defined based on experience and estimation.

(2) Collector Sectional Area: Considering the physical characteristics of S/S, the thickness of the microchannel generally does not exceed 3.5 mm [44] after stamping. The L was kept constant at 23.7 mm. Therefore, the values of H and D were varied and optimized to improve collector performance. The mesh generation was accomplished using Tet/Hybrid in TGrid, and an interval size of 1 was defined based on experience and estimation. Detailed parameters for H and D are provided in Table 1.

These variations in collector diameter and sectional area allow for a comprehensive analysis of performance and optimization possibilities..

2.3. Thermodynamic description

The medium in S/S FPSC was antifreeze, which is a non-compressible fluid. Its flow was driven by forced power from a pump. The heat transfer in S/S FPSC is governed by RNG k-ε turbulence model equations shown in equations (1) and (2).

$$\frac{\partial(\rho k u_i)}{\partial x_i} = \frac{\partial}{\partial x_j}\left[\left[\mu + \frac{\mu_t}{\sigma_k}\right]\frac{\partial k}{\partial x_j}\right] + G_k - \rho\varepsilon \tag{1}$$

$$\frac{\partial(\rho \varepsilon u_i)}{\partial x_i} = \frac{\partial}{\partial x_j}\left[\left[\mu + \frac{\mu_t}{\sigma_\varepsilon}\right]\frac{\partial k}{\partial x_j}\right] + C_{1\varepsilon}\frac{\varepsilon}{k}G_k - C_{2\varepsilon}\rho\frac{\varepsilon^2}{k} \tag{2}$$

Where G_k represents the generation of turbulence kinetic energy due to the mean velocity gradients.

σ_k is the turbulent Prandtl number for turbulent kinetic energy(k).

σ_ε is the turbulent dissipation rate(ε).

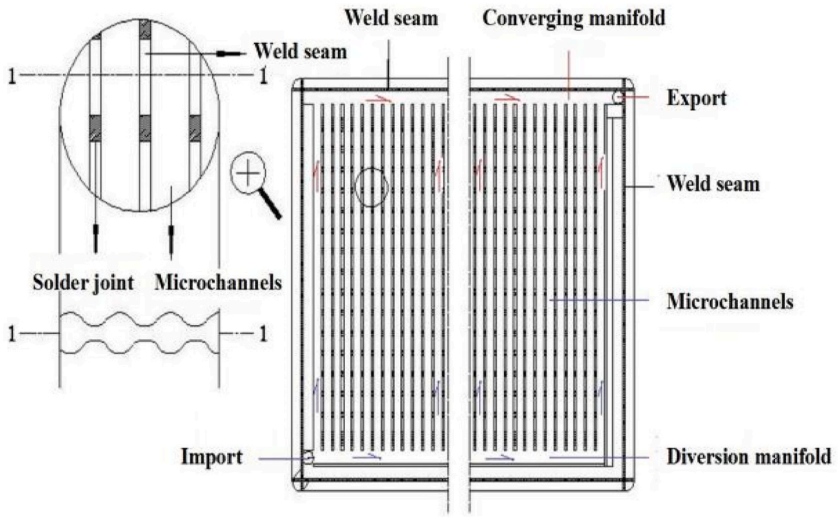

Fig. 2. The structure of S/S FPSCs.

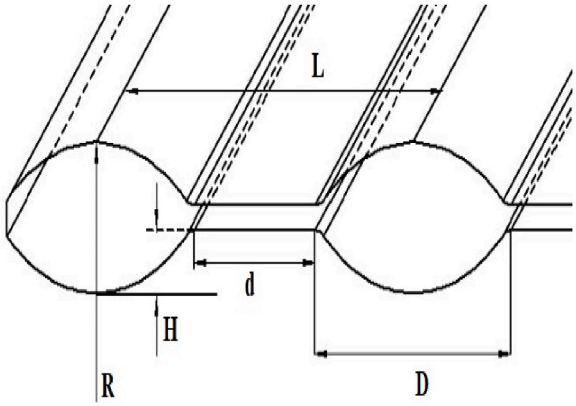

Fig. 3. The section picture of S/S FPSCs.

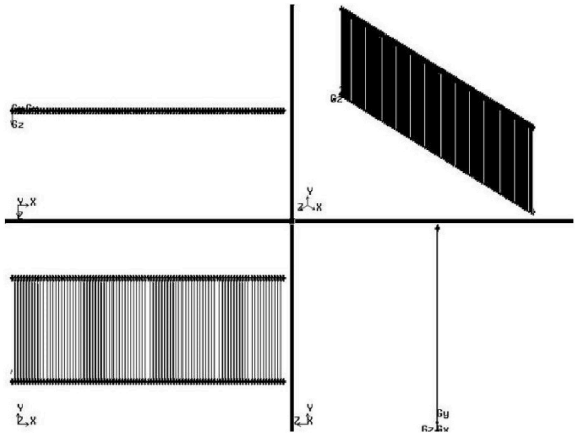

Fig. 4. The 3D model in a coordinate system.

Table 1
The sectional area of collectors.

Models	Parameters of models/(mm)	
	H	D
1	2.5	7.7
2	2.5	8.7
3	2.5	10.7
4	2.5	11.7
5	2	9.7
6	2.25	9.7
7	2.75	9.7
8	3	9.7
9	2.5	9.7

$C_{1\varepsilon}$, $C_{2\varepsilon}$ are two constants for the turbulent model: $C_{1\varepsilon}$, $= 1.44$, $C_{2\varepsilon} = 1.92$, $\sigma_k = 1.0$,$\sigma_\varepsilon = 1.3$.

The collector surface of S/S also serves as the heat exchange surface for the medium, and the temperature of the collector surface is equal to the heat source temperature during heat exchange. Considering the collector as a whole object, the heat transfer analysis of the microchannel includes two main parameters: heat transfer in the system(φ) and average heat transfer coefficient(α), as shown in equations (3) and (4).

$$\varphi = mC_p(t'' - t') \tag{3}$$

$$\alpha = \frac{\varphi}{(T - t)F} \tag{4}$$

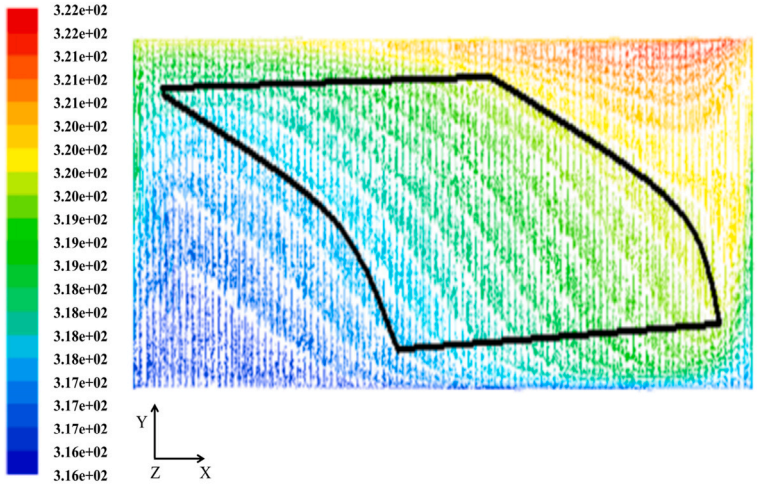

(a) 6 mm diameter

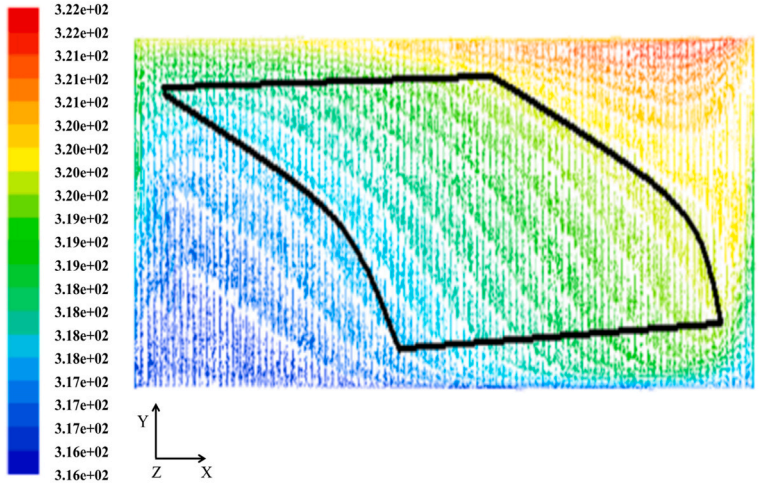

(b) 7 mm diameter

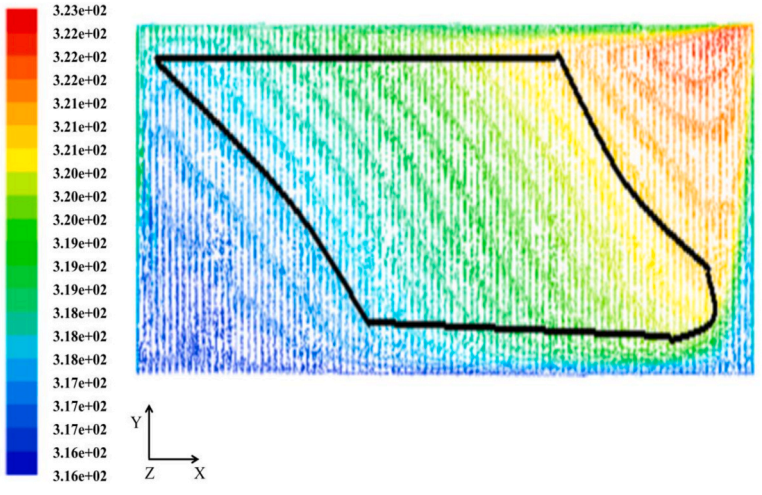

(c) 8 mm diameter

(caption on next page)

Fig. 5. Temperature contours in channels with different diameter.

Where m (kg/s) is the mass flow rate of the heat transfer fluid.

t' (°C) is the outlet temperature.

t'' (°C) is the inlet temperature.

T (°C) is the surface temperature.

t (°C) is the steady-state temperature of the medium.

F (m^2) is the heat transfer area of the collector.

The Nusselt number is a critical parameter that provides insights into the convective heat transfer characteristics of the system under steady-state conditions. When the medium in the collector stays in a steady state, the Nusselt number indicates the intensity of heat transfer, as shown in equation (5).

$$N_u = \frac{\alpha D_e}{\lambda} = a' R_e^{b'} P_r^m = a R_e^{\ b} \tag{5}$$

Where λ [W/(m·K)]is the thermal conductivity of the medium.

a, b are unknown parameters.

Re is Reynolds number.

Pr is Prandtl number.

The resistance equation is shown in equation (6)

$$f = \frac{-(dp/dx)D_e}{\rho u_m^2/2} = c R_e^{\ d} \tag{6}$$

The equivalent diameter of the microchannel is defined by equation (7), shown in the following equation.

$$D_e = \frac{4A}{U} \tag{7}$$

Where A (m^2) is the area section of the microchannel.

U (m) is the perimeter of the microchannel.

The size of the microchannels in our study is significantly smaller than that of traditional heat exchangers. Kandlikar [45] defined channels with dimensions ranging from 10 μm to 200 μm as microchannels. In our study, the size of our microchannels falls between that of typical heat exchangers and microchannels, as per Kandlikar's definition. Therefore, this study draws upon previous experiences and research as reference points for comparison. This positioning provides a context for understanding the unique characteristics and challenges associated with the microchannels in our collector design.

The mathematical characterization of fluid flow and heat transfer used in our model for the microchannel heat-absorbing plate is highly accurate. It serves as a valuable predictive reference for future developments and optimizations in microchannel heat-absorbing plate technology. The precision of our model contributes to its reliability as a tool for understanding and advancing microchannel heat-absorbing plate designs, paving the way for further innovations in this technology.

3. Simulation results and parameter determination

3.1. Experimental verification

This study configured all parameters, including solar radiation, inlet temperature, inlet flow rate, and collector structure, in Gambit to reflect actual working conditions. Following the simulation, the outlet temperature of the heat exchange medium was calculated to be 320 °C, closely matching the experimental results of 320.5 °C. This comparison demonstrates that the numerical model's results align almost perfectly with the experimental findings. The deviation in the outlet temperature was only 0.2%, confirming the validity and accuracy of our simulation model. This high level of agreement between simulation and experimentation enhances the confidence in the model's predictive capabilities.

3.2. Temperature contours

Fig. 5 displays temperature profiles within the length-width interface of the channels, each having different diameters: 6 mm, 7 mm, and 8 mm. These profiles can be categorized into three distinct zones characterized by isotherms: the diffusion zone, stability zone (represented by the black range), and contraction zone. These zones exhibit a direct correlation with the properties of the heat transfer medium [20]. To be specific, in the diffusion zone, the inlet temperature remains at a lower level (indicated by the blue zone), with a gradual rate of temperature increase. Because of the uniform distribution of thermal conduction, the efficiency of heat transfer experiences a notable improvement within the stability zone. In the contraction zone, temperatures are consistently at relatively high levels (shown in the red zone). This analysis provides insights into the temperature distribution and heat transfer efficiency across different zones of the collector channels with varying diameters.

Within this uniform distribution zone of heat flow density, thermal resistance is minimal, and flow stagnation areas are absent, resulting in elevated temperatures on a small scale. Observing the temperature patterns, this work shows that expanding the stability zone while diminishing the diffusion and contraction zones represents an effective strategy to enhance thermal conduction efficiency within this absorber plate. In essence, optimizing the size of the microchannels or adjusting operating parameters can lead to performance improvements in the collectors.

Fig. 6 illustrates the temperature distribution between channels, highlighting temperature variations and heat exchange efficiency. Noticeable temperature differences are observed within the channels. This phenomenon occurs as the medium flows through the channels, creating vortex disturbances that disrupt the heat transfer boundary layer, ultimately enhancing the overall heat transfer effect.

3.3. Heat transfer characterization

Based on the thermodynamic description, the parameters *f*, *Nu* are defined by constants *a*, *b*, *c*, and *d*. Table 2 shows the constants *a*, *b*, *c*, and *d* in 9 different structure sizes, which were put into a heat equation to show the relationship between *Re*, *Nu* and *f*.

This research conducted a comparative analysis to illustrate the relationship between Re and *f*. Initially, this study maintained *H* at 2.50 mm while varying D from 7.70 mm to 11.70 mm. As shown in Fig. 7(a,b), there is a trend of initially increasing and then decreasing as *D* increases. When *D* reached 8.70 mm, the flow resistance *f* reached its peak value, signifying the maximum heat exchange efficiency. Fig. 7(c,d) shows the change trend with *H* as the counterpart. When keeping *D* constant at 9.70 mm, this work explored a range of values for *H,* spanning from 2.00 mm to 3.00 mm. In this scenario, *f* exhibited an upward trend with variations in *H*. When *H* was 3.00 mm, the most effective heat transfer was achieved. Consequently, the optimal performance for the microchannel is achieved when *D* is 8.70 mm, and *H* is 3.00 mm.

Hence, by optimizing the microchannel width to 8.70 mm(*D*) and the height of corrugations to 3.00 mm(*H*), this work has achieved the most effective heat exchange performance. Accordingly, the product was manufactured according to these parameters. This successful optimization based on the analysis further validates the importance of careful tuning of microchannel dimensions for maximizing heat exchange efficiency in the collector design.

4. Experimental configuration in new product development

4.1. Product development

Solar selective coating(SSC) exhibits high absorption(α) within the range of 0.3–2.5 μm and low thermal emittance (*e*) [46]. Ultra-pure ferritic stainless steel(UFSS) is a new type of steel which has extremely low carbon and nitrogen content. UFSS [47] contains high levels of Cr(13–30%), low amounts of Ni and virtually no carbon or nitrogen elements. The combination of SSC and UFSS in the collector design contributes to optimal absorption and minimal thermal emittance, enhancing the overall efficiency of the solar collector.

Additionally, trace elements like Mo and Nb are developed explicitly for UFSS. In comparison to Austenitic Stainless Steel (ASS), SFSS offers significant advantages in solar thermal applications. These advantages include higher thermal conductivity, enhanced corrosion resistance, and reduced susceptibility to work hardening. The tailored composition of UFSS makes it a favourable material for solar thermal collectors, ensuring improved performance and durability in harsh environmental conditions.

TTS445J1, a typical UFSS, serves as a substrate for our application. By improving the chemical coloring process for SSC, the solar absorber gains several advantages, including excellent durability, cost-effectiveness, and high performance [48]. The coloring solution incorporates $ZnSO_4$, $Cr_2(SO_4)_3$, and other additives to $Na_2Cr_2O_7$–H_2SO_4, which are heated and applied to the surface to form the SSC.

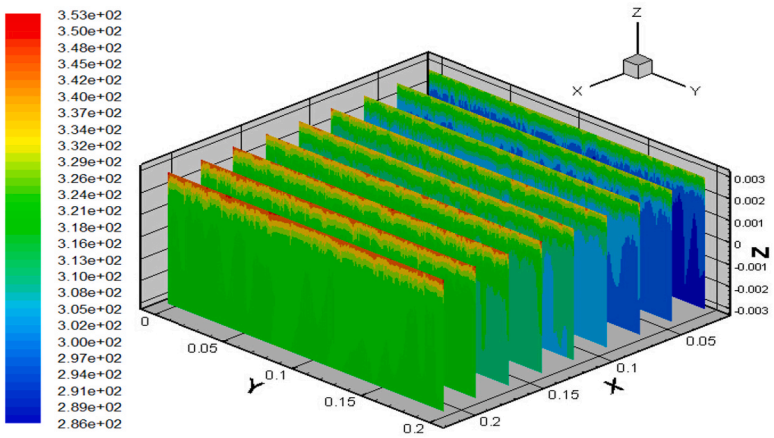

Fig. 6. Temperature distribution of medium between channel.

Table 2
The constant *a*, *b*, *c*, *d*.

Models (H × D/mm)	*a*	*b*	*c*	*d*
1 (2.5 × 7.7)	1.6576	0.4911	86.8003	0.5172
2 (2.5 × 8.7)	1.3688	0.5273	66.7564	0.4684
3 (2.5 × 10.7)	1.4520	0.4941	77.0034	0.5377
4 (2.5 × 11.7)	1.5272	0.4816	93.6796	0.5921
5 (2 × 9.7)	1.4934	0.4879	93.2263	0.6121
6 (2.25 × 9.7)	1.4729	0.4971	98.1248	0.5919
7 (2.75 × 9.7)	1.6754	0.4892	90.5833	0.5122
8 (3 × 9.7)	1.8311	0.4823	92.6075	0.4840
9 (2.5 × 9.7)	1.7728	0.4670	114.8549	0.6004

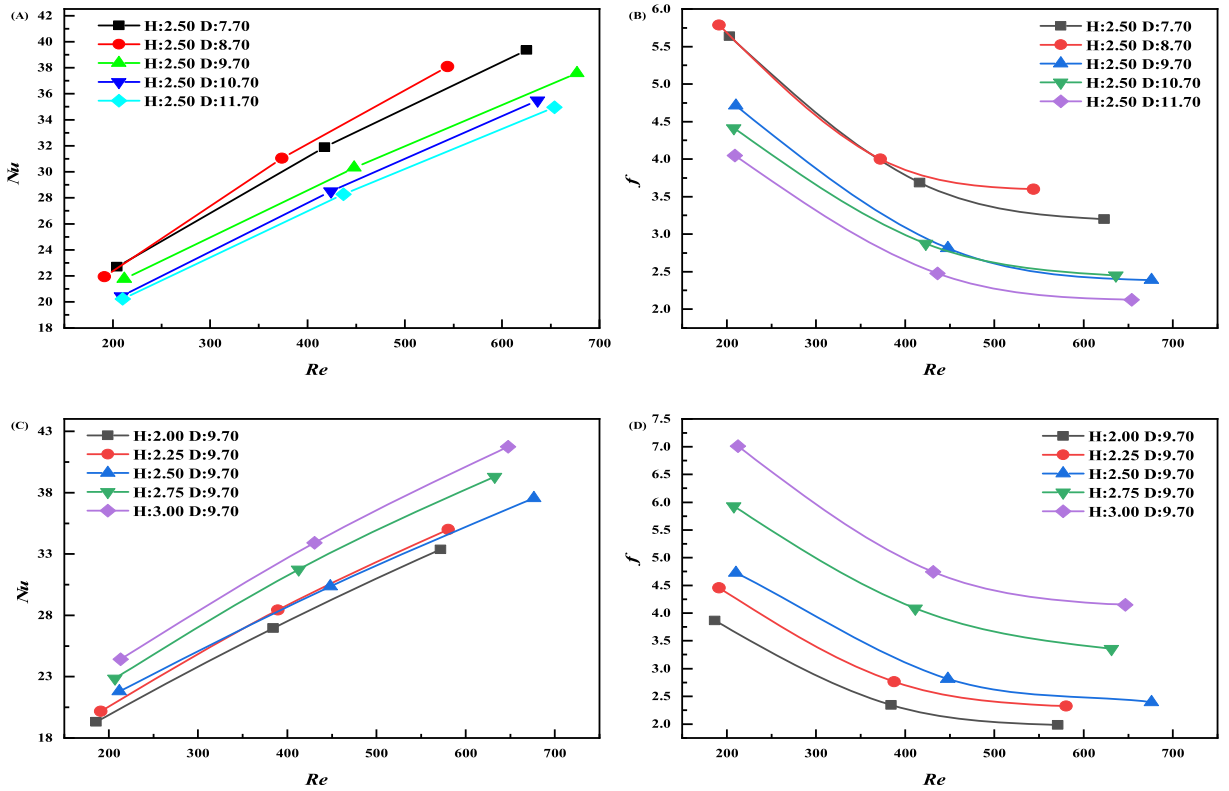

(a) The changes of *Nu*, *Re* under different *D*,(b) The changes of *f* under different *D*;
(c) The changes of *Nu*, *Re* under different *H*, (d) The changes of *f* under different *H*;

Fig. 7. The changes of flow parameter over the size of airflow.

Based on wall installation requirements, the collector is designed with dimensions of 2370×800 mm and a thickness of 0.41 mm, ensuring compatibility with most building window spaces.

These collectors are created by stamping them out from a roll of S/S using a mold designed for semi-arc channel formation. Two semi-arc channels are interlocked to produce a complete channel structure. The frames are securely encapsulated through welding, and additional soldering between each channel enhances the collector's pressure-bearing capacity. The heat transfer medium enters the micro-channel from the inlet, where it is heated by sunlight irradiation. It then flows upward through siphonage and is transferred to the hot water storage tank through the outlet. This detailed description provides an overview of the materials, manufacturing process, and operational aspects of the solar collector.

4.2. Experimental configuration

The products fabricated and evaluated in this study were set in Ji'nan as the location for testing, which provides a real-world

scenario for evaluating the collector's performance under specific environmental conditions. This study examines the thermal performance of the new solar collector. The test environment follows the Test Methods for Solar Collectors. Table 3 describes the details of the S/S FPSC. The frame structure was set in an outdoor environment.

The schematic diagram of the experimental setup and the placement of sensors are depicted in Fig. 8. Each serial number corresponds to specific instruments and measurement points. The test of the solar collector involves two crucial steps: the heat collection cycle and data measurement.

During the heat collection cycle, a secondary motion for heat transfer was incorporated, with propylene glycol in water serving as the heat transfer medium. Circulating pumps provided the necessary cyclic power. The measured data encompasses parameters such as the inlet and outlet temperatures of the heat collector, the water temperature in the tank, the flow rate of the medium, solar radiation intensity, environmental temperature, and wind speed. Table 4 provides an overview of the measurement parameters and the corresponding measuring instruments. Fig. 8 offers a visual representation of the experimental setup and measurement points.

5. Results and discussion

5.1. Assessment of gathered data

The collected data, primarily temperature measurements, will be presented and analyzed in graphical form. As part of this study, new solar modules for performance testing was conduct in real-world conditions, and the results are displayed in Fig. 9. Furthermore, the performance of the new product was validated by simulating the new solar module in Fluent as a control group, as depicted in Fig. 9.

From these figures, this study found.

(1) Both sets of results exhibit consistent temperature trends, which can be attributed to similar meteorological conditions, including solar radiation intensity, wind speed, and environmental temperature. Consequently, the test platform for FPSCs proves to be valid for assessing the performance of solar modules.
(2) Solar radiation intensity demonstrates a steady increase before reaching its peak around high noon. During this period, the inlet and outlet temperatures of the micro-channel collector, as well as the water temperature in the tank, exhibit linear growth in direct correlation with the solar radiation intensity.
(3) As solar radiation intensity reaches its peak and subsequently experiences a significant decline, the inlet and outlet temperatures of the micro-channel collector remain at high levels. These temperatures continue to exhibit a slight upward trend until the temperature difference between them reaches its minimum value.

The results indicate that the micro-channel collector exhibits a high heat-collecting capacity and superior thermal insulation. It effectively converts light energy into heat energy through the flow of the medium, facilitating efficient heat utilization. The consistent temperature trends and correlation with solar radiation intensity validate the performance of the solar modules and highlight the effectiveness of the micro-channel collector in efficient heat conversion.

5.2. Efficiency estimation

During the experiment, the collector operated consistently. From the diagram of the collected data, this study selected data that exhibited a gradual upward trend during a specific time period (10:15–12:00). During this period, the solar radiation intensity remained at or above 700 W/m^2, and the surrounding air velocity did not exceed 4 m/s. The details are shown in Table 5.

There exists a relationship between changes in water temperature and solar radiation. To illustrate the temperature difference over time during the solar heating phase, this study introduces the Normalized Difference Temperature Index (NDTI), which quantifies the change in temperature per unit of solar radiation. This research employed curve-fitting techniques to calculate the momentary

Table 3
S/S FPSC details.

Details	Measure data
Absorber plate alloy	S/S(TTS445J1)
Dimensions of absorber	
Length	2370 mm
Width	800 mm
Thickness	0.41 mm
Fluid coolant	Air
Dimensions of Air duct	
Type	Microchannel
Shape	Ellipse
Width	8.70 mm
Height	3.00 mm
Air duct spacing	1.00 mm
Tube alloy	S/S(TTS445J1)

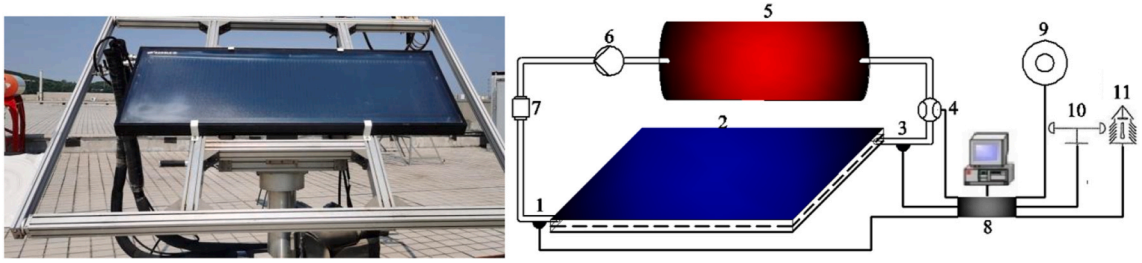

Fig. 8. Schematic diagram of the experiment setup and measure point.

Table 4
The measurement parameters and measuring apparatus.

Sensor	Used to measure	Uncertainty	Specification
Pyranometer	Solar radiation	$< \pm 2\%$	TBQ-2, Jinzhou Sunshine Development Co., Ltd, China
Temperature sensor	Inlet and outlet water temperature	$\pm 0.3\ ^{\circ}C$	PT100 WZPM-201, Anhui Tiankang (Group) Co., Ltd, China
Mass Flow Meter	Control mass flow of heat exchange medium	$\pm 0.5\%$	US211 M, Shandong Xinzhun Electronic Technology Co., Ltd, China
Anemometer	Wind speed	$\pm 5\%$	AT816, SMART SENSOR, China

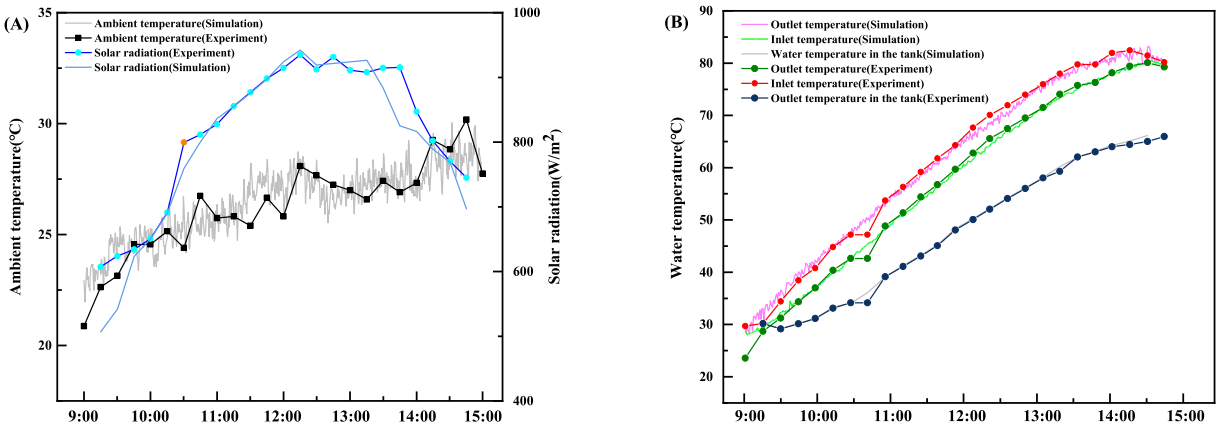

(a) The simulation and measured value of solar radiation intensity and ambient temperature

(b)The water temperature of the collector's different positions

Fig. 9. Gathered data.

Table 5
The gathered data from the experiment.

Time	Inlet temperature T_i/(°C)	Outlet temperature T_o/(°C)	Ambient temperature T_e/(°C)	Solar radiation I/(W/m^2)	Mass flow m/(kg/h)	NDTI	Efficiency
10:15	42.63	47.17	24.40	799.47	307.2	0.022883	76.30%
10:30	45.99	50.69	26.74	811.57	307.2	0.023792	75.21%
10:45	48.85	53.72	25.74	827.72	317.4	0.028029	79.62%
11:00	51.37	56.32	25.82	855.55	314.4	0.030151	74.33%
11:15	54.39	59.18	25.40	877.09	318	0.033101	73.09%
11:30	56.74	61.78	26.66	898.18	319.2	0.033972	72.22%
11:45	59.68	64.30	25.82	914.77	313.2	0.036968	71.13%
12:00	62.79	67.66	28.09	934.97	313.2	0.037711	68.16%

efficiency of S/S FPSCs under different surrounding conditions. This detailed analysis allows for a deeper understanding of the collector's performance under specific operational and environmental conditions.

Considering the information provided in the preceding figures, Fig. 10 illustrates the fitted line, depicting the correlation between NDTI and momentary efficiency with respect to the inlet temperature. The ultimate expression of the equation is articulated below:

$$\eta = 0.86101 - \frac{4.17863(T_i - T_e)}{I} \tag{8}$$

Sun [49] employed the same method to analyze the theoretical maximum instantaneous efficiency variation pattern of collectors in cold regions and obtained similar trends in the variations. Irshad [50] discovered a fitted line enabling the calculation of the effective optical efficiency of a single-pass flat plate solar collector, reaching up to 72.7%. Jalil [40] utilized the micro-channel technique to enhance the performance of a solar collector, achieving the highest thermal efficiency of 72.8% and practical efficiency of 70.44%, respectively. While previous studies did not attain such elevated efficiency levels, the observed trend remains consistent. The nuanced variations in flow channel structure engender substantial disparities in efficiency, thereby validating the superiority of this specific flow channel configuration from an academic perspective.

5.3. Limitations

This study aims to develop a new solar collector using simulation software to determine optimal structural dimensions for maximizing energy efficiency. Through summarizing and analyzing the study, limitations emerge that can guide future research directions.In this type of optimization design, the distribution of airflow within the collector flow path becomes more complex, resulting in pressure loss that ultimately impacts efficiency. Jia [51] optimized the flow channels, reducing pressure loss to 37.26% of the original and increasing efficiency by 2.18%. In future work, these researches aim to establish the relationship between flow rate, pressure loss, and efficiency to further explore optimization methods. Meanwhile, environmental and economic assessments of S/S FPSCs pose limitations. An analogous study conducted by Anindita and Partha [52] examined the economic and energy payback periods of a solar air heater. Abo-Elfadl et al. [53] conducted a similar assessment on a new absorber, demonstrating carbon credit earnings of $561.9/year. Economic research reveals variations in economic benefits among solar collectors due to different application scenarios. Dutta et al. [54] enhanced a solar dryer for drying local seasonal medicinal fruit, yielding significant economic benefits with economic payback periods of approximately one year. Similar conclusions were drawn in the field of tea drying [55,56], emphasizing the effectiveness of low-temperature drying methods for tea processing. The exergy analysis can be enhanced by a more comprehensive examination of the utilization of helpful energy within the system. Bahrehmand [57] identified a more efficient solar air collector system by comparing various collectors through exergy analysis.

6. Conclusion

A novel design of a Stainless Steel Flat Plate Solar Collector (S/S FPSC) featuring full-flow channels has been developed to enhance its thermal performance through the introduction of micro-channel stamping. In this study, the accuracy of the mathematical model was validated using a simulation program, accounting for specific climate conditions in Ji'nan. The key findings from the design and experimentation processes are as follows.

(1) The structure of the FPSC was optimized, with Stainless Steel (TTS445J1) selected as the substrate material, considering specific feature sizes.
(2) The finished S/S FPSCs exhibited temperature uniformity and improved durability, attributed to the use of Stainless Steel (TTS445J1).
(3) A mathematical expression has been developed to establish the relationship between surrounding conditions and the momentary efficiency of S/S FPSCs. Under these conditions, the projected momentary efficiency is an impressive 86.10%.

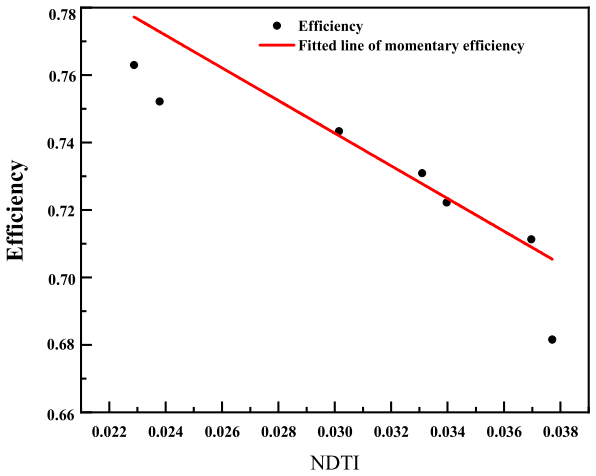

Fig. 10. Normalized fitted curve based on the inlet temperature.

In summary, this research successfully implements a new design for an S/S FPSC, resulting in enhanced thermal performance, temperature uniformity, and increased durability. Additionally, the developed mathematical model provides valuable insights into the connection between surrounding conditions and the momentary efficiency of the solar collector.

Data availability statement

The dataset supporting the findings of this study is available from the corresponding author upon reasonable and justified request.

CRediT authorship contribution statement

Yi He: Writing – review & editing, Writing – original draft. **Hongwen Yu:** Supervision, Project administration, Methodology, Investigation, Data curation. **Guangbin Duan:** Resources, Investigation. **Yong Wang:** Software, Data curation. **Qianfu Yang:** Resources. **Lei Feng:** Resources. **Jiaming Zhang:** Resources.

Declaration of competing interest

The authors declare that they have no known competing financial interests or personal relationships that could have appeared to influence the work reported in this paper.

Acknowledgements

This work was supported by Key Research and Development Program of Shandong Province (2023RZA02020); Science and Technology SMEs Innovation Capacity Enhancement Project of Shandong Province (No. 2022TSGC2144, 2022TSGC2322, 2023TSGC0986); Natural Science Foundation of Shandong Province (ZR2021ME185); Shandong Innovation and Entrepreneurship Community for Carbon Peaking and Neutrality in Construction & Traffic Industry (No. STGTT0101202303, STGTT0101202302).

References

[1] G. Colangelo, E. Favale, P. Miglietta, A. De Risi, Innovation in flat solar thermal collectors: a review of the last ten years experimental results, Renew. Sustain. Energy Rev. 57 (2016) 1141–1159.
[2] A. El-Sawi, A. Wifi, M. Younan, E. Elsayed, B. Basily, Application of folded sheet metal in flat bed solar air collectors, Appl. Therm. Eng. 30 (8–9) (2010) 864–871.
[3] L. Evangelisti, R.D.L. Vollaro, F. Asdrubali, Latest advances on solar thermal collectors: a comprehensive review, Renew. Sustain. Energy Rev. 114 (2019) 109318.
[4] G. Li, Q. Xuan, M. Akram, Y.G. Akhlaghi, H. Liu, S. Shittu, Building integrated solar concentrating systems: a review, Appl. Energy 260 (2020) 114288.
[5] T. Beikircher, P. Osgyan, M. Reuss, G. Streib, Flat plate collector for process heat with full surface aluminium absorber, vacuum super insulation and front foil, Energy Proc. 48 (2014) 9–17.
[6] L.S. Sundar, A. Kirubeil, V. Punnaiah, M.K. Singh, A.C. Sousa, Effectiveness analysis of solar flat plate collector with Al2O3 water nanofluids and with longitudinal strip inserts, Int. J. Heat Mass Tran. 127 (2018) 422–435.
[7] E.M. Abo-Zahhad, S. Memon, A. Radwan, M.R. Elmarghany, A. Khater, C. Ghenai, O. Abdelrehim, A new fusion-edge sealed vacuum for concentrated photovoltaic/thermal solar collector in comparison to a conventional system, Case Stud. Therm. Eng. 34 (2022) 102003.
[8] F. Giovannetti, S. Föste, N. Ehrmann, G. Rockendorf, High transmittance, low emissivity glass covers for flat plate collectors: applications and performance, Sol. Energy 104 (2014) 52–59.
[9] S. Mekhilef, R. Saidur, A. Safari, A review on solar energy use in industries, Renewable and sustainable energy reviews 15 (4) (2011) 1777–1790.
[10] B. Jia, L. Yang, L. Zhang, B. Liu, F. Liu, X. Li, Optimizing structure of baffles on thermal performance of spiral solar air heaters, Sol. Energy 224 (2021) 757–764.
[11] Z. Song, Y. Xue, B. Jia, Y. He, Introduction of the rectangular hole plate in favor the performance of photovoltaic thermal solar air heaters with baffles, Appl. Therm. Eng. 220 (2023) 119774.
[12] S. Sobhansarbandi, P.M. Martinez, A. Papadimitratos, A. Zakhidov, F. Hassanipour, Evacuated tube solar collector with multifunctional absorber layers, Sol. Energy 146 (2017) 342–350.
[13] A. Fernández, J. Dieste, Low and medium temperature solar thermal collector based in innovative materials and improved heat exchange performance, Energy Convers. Manag. 75 (2013) 118–129.
[14] T. Beikircher, M. Möckl, P. Osgyan, G. Streib, Advanced solar flat plate collectors with full area absorber, front side film and rear side vacuum super insulation, Sol. Energy Mater. Sol. Cell. 141 (2015) 398–406.
[15] Z. Chen, M. Gu, D. Peng, Heat transfer performance analysis of a solar flat-plate collector with an integrated metal foam porous structure filled with paraffin, Appl. Therm. Eng. 30 (14–15) (2010) 1967–1973.
[16] B. Jia, F. Liu, X. Li, A. Qu, Q. Cai, Influence on thermal performance of spiral solar air heater with longitudinal baffles, Sol. Energy 225 (2021) 969–977.
[17] D. De Luca, A. Caldarelli, E. Gaudino, E. Di Gennaro, M. Musto, R. Russo, Modeling of energy and exergy efficiencies in high vacuum flat plate photovoltaic–thermal (PV–T) collectors, Energy Rep. 9 (2023) 1044–1055.
[18] H. Panchal, A. Sohani, N. Van Nguyen, S. Shoeibi, M. Khiadani, P.Q. Huy, S. Hoseinzadeh, A.E. Kabeel, S. Shaik, E. Cuce, Performance evaluation of using evacuated tubes solar collector, perforated fins, and pebbles in a solar still–experimental study and CO2 mitigation analysis, Environ. Sci. Pollut. Control Ser. 30 (5) (2023) 11769–11784.
[19] T.C. Diamantino, R. Gonçalves, A. Nunes, S. Páscoa, M.J. Carvalho, Durability of different selective solar absorber coatings in environments with different corrosivity, Sol. Energy Mater. Sol. Cell. 166 (2017) 27–38.
[20] R.W. Moss, P. Henshall, F. Arya, G. Shire, P.C. Eames, T. Hyde, Simulator testing of evacuated flat plate solar collectors for industrial heat and building integration, Sol. Energy 164 (2018) 109–118.
[21] G. Nanajkar, P. Eames, Finite Element Analysis of a Novel Building Integrated Solar Thermal Vacuum Flat Plate Collector for Water and Space Heating, 2019.
[22] H. Yu, X. Xu, Y. Zhang, Q. Zhang, G. Li, H. Yan, Preparation of high corrosion resistant solar absorbing coating on the surface of ferritic stainless steel by utilizing chemical coloring, Mater. Lett. 270 (2020) 127628.
[23] C.S. Peixoto, M. Teles Neto, Y. Shigaki, NNd Silva, W. Sade, Electrolytic deposition of ni/nio on stainless steel for production of selective surfaces, Mater. Res. 24 (2021).
[24] S. Wu, C.-H. Cheng, Y.-J. Hsiao, R.-C. Juang, W.-F. Wen, Fe2O3 films on stainless steel for solar absorbers, Renew. Sustain. Energy Rev. 58 (2016) 574–580.

[25] C. Yuan, M. Li, M. Wang, Y. Dan, T. Lin, H. Cao, M. Zhang, P. Zhao, H. Yang, Electrochemical development and enhancement of latent fingerprints on stainless steel via electrochromic effect of electrodeposited Co3O4 films, Electrochim. Acta 370 (2021) 137771.
[26] Q. Su, S. Chang, C. Yang, Loop heat pipe-based solar thermal façade water heating system: a review of performance evaluation and enhancement, Sol. Energy 226 (2021) 319–347.
[27] E. Vengadesan, R. Senthil, A review on recent developments in thermal performance enhancement methods of flat plate solar air collector, Renew. Sustain. Energy Rev. 134 (2020) 110315.
[28] J. Ma, W. Sun, J. Ji, Y. Zhang, A. Zhang, W. Fan, Experimental and theoretical study of the efficiency of a dual-function solar collector, Appl. Therm. Eng. 31 (10) (2011) 1751–1756.
[29] K. Chong, K. Chay, K. Chin, Study of a solar water heater using stationary V-trough collector, Renew. Energy 39 (1) (2012) 207–215.
[30] R. Kumar, E. Cuce, S. Kumar, S. Thapa, P. Gupta, B. Goel, C.A. Saleel, S. Shaik, Assessment of the thermo-hydraulic efficiency of an indoor-designed jet impingement solar thermal collector roughened with single discrete arc-shaped ribs, Sustainability 14 (6) (2022) 3527.
[31] T. Wang, Y. Diao, Y. Zhao, L. Liang, Z. Wang, C. Chen, A comparative experimental investigation on thermal performance for two types of vacuum tube solar air collectors based on flat micro-heat pipe arrays (FMHPA), Sol. Energy 201 (2020) 508–522.
[32] J.-S. Yu, J.-H. Kim, J.-T. Kim, Effect of triangular baffle arrangement on heat transfer enhancement of air-type PVT collector, Sustainability 12 (18) (2020) 7469.
[33] S. Gholipour, M. Afrand, R. Kalbasi, Improving the efficiency of vacuum tube collectors using new absorbent tubes arrangement: introducing helical coil and spiral tube adsorbent tubes, Renew. Energy 151 (2020) 772–781.
[34] A. Kotb, M.B. Elsheniti, O.A. Elsamni, Optimum number and arrangement of evacuated-tube solar collectors under various operating conditions, Energy Convers. Manag. 199 (2019) 112032.
[35] X. Li, Y. Dai, Y. Li, R. Wang, Comparative study on two novel intermediate temperature CPC solar collectors with the U-shape evacuated tubular absorber, Sol. Energy 93 (2013) 220–234.
[36] R. Joshi, R. Chhibber, High temperature wettability studies for development of unmatched glass-metal joints in solar receiver tube, Renew. Energy (2018). S0960148117312168.
[37] J.C. Gomez-Vidal, J. Noel, J. Weber, Corrosion evaluation of alloys and MCrAlX coatings in molten carbonates for thermal solar applications, Sol. Energy Mater. Sol. Cell. 157 (2016) 517–525.
[38] P.P. Dutta, H. Kakati, M. Bardalai, P.P. Dutta, Performance studies with trapezoidal, sinusoidal and square corrugated aluminium alloy (AlMn1Cu) plate ducts, Modeling, simulation and optimization (2021) 751–774. Proceedings of CoMSO 2020. Springer.
[39] X. Gong, F. Wang, H. Wang, J. Tan, Q. Lai, H. Han, Heat transfer enhancement analysis of tube receiver for parabolic trough solar collector with pin fin arrays inserting, Sol. Energy 144 (2017) 185–202.
[40] J.M. Jalil, N.A. Abdulkadhim, Effect of micro-channel technique on solar collector performance, in: IOP Conference Series: Materials Science and Engineering, vol. 518, IOP Publishing, 2019 032047.
[41] J.M. Jalil, G.A. Aziz, A.A. Kadhim, Heat transfer enhancement in air duct flow by micro-channel experimental and numerical investigation, in: IOP Conference Series: Materials Science and Engineering, vol. 765, IOP Publishing, 2020 012027.
[42] Y. Wang, The Experimental Study and Numerical Simulation of Microchannel Flat Solar Collector Fluid Heat Collecting, University of Ji'nan, 2016.
[43] X. Liu, Experimental Research and Simulation Analysis of Microchannel Solar Collector Thermal Performance, Shandong University of Science and Technology, 2020.
[44] Dolores B. Amaya, A. Ruiz Flores, A. Núñez Galindo, J.J. Calvino Gámez, J.F. Almagro, L. Lajaunie, Textural, microstructural and chemical characterization of ferritic stainless steel affected by the gold dust defect, Materials 16 (5) (2023) 1825.
[45] S. Kandlikar, S. Garimella, D. Li, S. Colin, M.R. King, Heat Transfer and Fluid Flow in Minichannels and Microchannels, elsevier, 2005.
[46] T. Kittessa, Roro, Tile Ngcali, Mwakikunga Bonex, Solar absorption and thermal emission properties of multiwall carbon nanotube/nickel oxide nanocomposite thin films synthesized by sol–gel process, Materials Science & Engineering B (2012).
[47] L. Ma, J. Han, J. Shen, S. Hu, Effects of microalloying and heat-treatment temperature on the toughness of 26Cr–3.5 Mo super ferritic stainless steels, Acta Metall. Sin. 27 (2014) 407–415.
[48] H. Yu, X. Xu, Y. Zhang, Q. Zhang, H. Yan, Preparation of high corrosion resistant solar absorbing coating on the surface of ferritic stainless steel by utilizing chemical coloring, Mater. Lett. 270 (2020) 127628.
[49] W. Sun, in: Cold RegionsMicro Heat Pipe Flat-Plate Solar CollectorMulti-Plate Efficiency Optimization of, Jilin Jianzhu University, 2021.
[50] M. Irshad, A. Yadav, R. Singh, A. Kumar, Mathematical modelling and performance analysis of single pass flat plate solar collector, in: IOP Conference Series: Materials Science and Engineering, vol. 404, IOP Publishing, 2018 012051.
[51] B. Jia, F. Liu, D. Wang, D. Zhang, T. Han, Optimization of flow path for the spoiler solar air collector, Chem. Ind. Eng. Prog. 38 (2) (2019) 7.
[52] A. Sharma, P.P. Dutta, Energy, exergy, economic and environmental (4E) assessments of a tea withering trough coupled with a solar air heater having an absorber plate with Al-can protrusions, Int. J. Ambient Energy 43 (1) (2022) 8438–8450.
[53] S. Abo-Elfadl, M.S. Yousef, H. Hassan, Energy, exergy, and enviroeconomic assessment of double and single pass solar air heaters having a new design absorber, Process Saf. Environ. Protect. 149 (2021) 451–464.
[54] P. Dutta, P.P. Dutta, P. Kalita, Thermal performance study of a PV-driven innovative solar dryer with and without sensible heat storage for drying of Garcinia Pedunculata, Environ. Sci. Pollut. Control Ser. (2023) 1–21.
[55] A. Sharma, P.P. Dutta, Evaluation of low-temperature drying characteristics of fresh tea leaves (Camellia assamica) in an environmental chamber using mathematical models, Res. Agric. Eng. 69 (2) (2023).
[56] A. Sharma, P.P. Dutta, Performance studies of low temperature solar drying of fresh tea leaves (camellia assamica), Appl. Sol. Energy 58 (3) (2022) 423–432.
[57] D. Bahrehmand, M. Ameri, Energy and exergy analysis of different solar air collector systems with natural convection, Renew. Energy 74 (2015) 357–368.